JUNO Calibration Strategy

someone[1)]

[1] School of Physics and Astronomy, Shanghai Jiao Tong University, Shanghai Key Laboratory for Particle Physics and Cosmology, Shanghai, 200240, China

Abstract: Jiangmen Underground Neutrino Observatory (JUNO) is a spherical neutrino detector with a target of 20 kton of liquid scintillator. It is located 700 m underground in Jiangmen, Guangdong Province, China. The primary goal of JUNO is to determine the neutrino mass hierarchy (MH). To accomplish this, the detector energy response is required to be highly linear (less than 1% uncertainty) with superior resolution (3% at 1 MeV). We discuss a comprehensive calibration strategy to achieve these requirements.

Key words: JUNO, Neutrino mass hierarchy, Calibration, Simulation, Radioactive sources, Double calorimetry

1 Introduction

The massive nature of neutrinos have been firmly established by the neutrino oscillation experiments [**?**]. However, the mass ordering of the three neutrino masses m_1, m_2, and m_3 remain unclear. The solar neutrino experiment has established that $m_2 > m_1$, but experimentally there has been no clear evidence whether m_3 is the largest or smallest of the three. This is so-called neutrino mass hierarchy (MH) problem.

The Jiangmen Underground Neutrino Observatory (JUNO) is a medium baseline reactor anti-neutrino detector, 53 km from the Yangjiang and Taishan nuclear power plants. The primary goal of this observatory is to use the electron anti-neutrino from the reactors to determine the neutrino mass hierarchy. Due to the neutrino oscillation, the survival probability of anti-neutrinos can be written as [**?**]:

$$P_{\overline{\nu_e}\to\overline{\nu_e}} = 1 - \sin^2 2\theta_{13} \times \left(\cos^2\theta_{12}\sin^2(\Delta m^2_{31}\frac{L}{4E_\nu}) + \sin^2\theta_{12}\sin^2(\Delta m^2_{32}\frac{L}{4E_\nu})\right) - \cos^4\theta_{13}\sin^2 2\theta_{12}\sin^2(\Delta m^2_{21}\frac{L}{4E_\nu}) \quad (1)$$

In this expression, θ_{12} and θ_{13} are the neutrino mixing angles, $\Delta m^2_{ij} \equiv m^2_i - m^2_j$ is the mass-square-difference between the mass eigenstates i and j, L is the distance from neutrino production to detection (baseline), and E_ν is the kinetic energy of the neutrino. Numerically, $|\Delta m^2_{32}|$ and $|\Delta m^2_{31}|$ are mostly degenerate ($\sim 2.5\times10^{-3}$ eV^2), Δm^2_{21} is much less with a value $\sim 7.5\times10^{-5}$ eV^2, and for the so-called normal or inverted hierarchy, $|\Delta m^2_{31}| = |\Delta m^2_{32}| \pm \Delta m^2_{21}$. Due to the lucky fact that $\theta_{12} \sim 30\,\mathrm{deg}$, the two oscillation frequencies are weighted differently, which allows one to determine the hierarchy given that the oscillation pattern can be measured with unprecedented high precision.

JUNO is a liquid scintillator (LS) detector with a mass of 20 kton, with a 12% mass of free protons. The LS is enclosed with a 35-m diameter acrylic sphere, strengthened by 591 stainless steel (SS) connection bars. ∼18000 20-in and ∼25000 3-in photomultipliers are immersed in ultrapure water outside the sphere viewing the LS. The electron anti-neutrinos are detected via the so-called inverse β-decay (IBD), $\bar{\nu}_e + p \to e^+ + n$,where the electron anti-neutrinos interact with protons from LS and then produce positrons and neutrons. The positron will deposit its kinetic energy in LS and at last will annihilate with an electron to produce two *gamma*s and the annihilation gammas will also deposit their kinetic energy in LS. The energy of the anti-neutrino is related to the positron energy, $E_{e+} \approx E_{\bar{\nu_e}}$ - 1.8 MeV, where E_{e+} and $E_{\bar{\nu_e}}$ are the kinetic energy of positron and electron anti-neutrino respectively. The neutron will be captured on a proton mostly with in about 200 *mu*s and produce a 2.2 MeV gamma as a delay signal. To determine the neutrino MH with high confidence sets very stringent requirements on the energy response of the detector. Specifically, the energy resolution of JUNO detector should be better than 3% at 1 MeV, and the uncertainty of the energy scale should be better than 1% [**?**]. These can only be achieved through a comprehensive calibration program.

Particle interactions in the liquid scintillator will produce scintillating (dominating) and Cerenkov (subdominant) photons. Although linear to the lowest order to the deposited energy, the scintillation photons has a known Birks' "quenching" effect [**?**] that depends on the energy loss (dE/dx), therefore producing an energy and particle dependent nonlinearity. Cerenkov photons are produced by a charged particle when its velocity exceeds the phase velocity of the light in the medium, which is clearly par-

1) E-mail: someone@sjtu.edu.cn

ticle dependent and nonlinear in energy. These photons will be converted to a charge readout by photomultiplier tubes (PMTs) and the downstream electronics chains. The intrinsic nonlinearity of the PMTs and the readout electronics would produce an additional nonlinearity to the energy measurement. We shall refer to these two effects as the "physics nonlinearity" and "electronics nonlinearity" hereafter, both should be independently calibrated and applied to physics events.

The other problem is the detector non-uniformity. For photons emitted at different interaction vertices, due to geometrical effects of the detector such as the optical transparencies of the LS, acrylic and water, reflections at boundaries of materials, shadowing due to non-transparent materials (e.g. SS connection bars), etc., the collection of the photons is clearly position dependent. Such non-uniformity, if not corrected, will worsen the energy resolution.

In this paper, we describe a comprehensive calibration strategy for JUNO, which consists of the following four complementary ingredients:

1. Multiple radioactive sources to calibrate physics nonlinearity;
2. Tunable photon source to calibrate electronics nonlinearity;
3. Many source locations to correct non-uniformity;
4. Redundancy using the so-called double calorimetry with two sets of PMTs.

We shall demonstrate, in the remainder of the paper, details of the strategy and how it satisfies the physics needs of JUNO.

2 Energy scale calibration

A JUNO custom Geant4-based (version 9.4.p04) [**?**] software, called SNIPER [**?**], is used to perform calibration related simulations. SNIPER consists of the up-to-date full detector geometries, optical properties, and physics lists which are selected and tuned based on the Daya Bay data.

2.1 Calibration of physics nonlinearity

2.1.1 Selection of sources

We select a wide range of γ sources ranging from a few hundred keV to a few MeV to cover the prompt energy range of the IBDs. ^{241}Am-Be and ^{241}Am-^{13}C are also used to both provide high energy gammas, as well as neutron capture signals. The sources are listed in Table. **??**.

Table 1. Radioactive sources

Source	Type	Radiation
^{137}Cs	γ	0.662 MeV
^{54}Mn	γ	0.835 MeV
^{60}Co	γ	1.173 + 1.333 MeV
^{40}K	γ	1.461 MeV
^{68}Ge	e^+	annil 0.511 + 0.511 MeV
^{241}Am-Be	n, γ	neutron + 4.43 MeV
^{241}Am-^{13}C	n, γ	neutron + 6.13 MeV

2.1.2 Model of energy nonlinearity

After an IBD reaction, the positron loses it energy by depositing ionization energy (the same way as an electron) before it stops *. Most of the positrons will immediately produce two annihilation 511 keV γs [**?**]. As a good approximation, a positron's visible total energy can therefore be written as

$$E^{e^+}_{vis} = E^{e}_{vis} + 2 \times E^{\gamma}_{vis}(511\ keV) \tag{2}$$

,where the first term describes the physics nonlinearity of an electron, and the second term can simply be measured by a source producing the two annihilation gammas (i.e. ^{68}Ge).

For demonstration purpose, the electron physics nonlinearity is modeled as an empirical four parameter function, as used in the Daya Bay data analysis [**?**],

$$\frac{E_{vis}}{E_{true}} = \frac{P_0 + P_3 E_{true}}{1 + P_1 e^{-P_2 E_{true}}}. \tag{3}$$

To determine these parameters, we apply the calibration data from various gamma sources as constraints, with the underlining physics that all gammas converts their energy via secondary electronic energy depositions, such as Compton scatterings, photoelectric effects, and pair production. For each gamma source, we use a MC to convert its gamma(s) to a probability density function (PDF) as a function of the energy of its secondary electrons. The measured gamma energy is simply the electron physics nonlinearity convolved with the PDF. With multiple sources, the parameters in Eqn. **??** can be determined. The quality of the fit to the gamma calibration data is illustrated in Fig. **??**.

*Simulations have shown that the effects of annihilation-in-flight can be neglected.

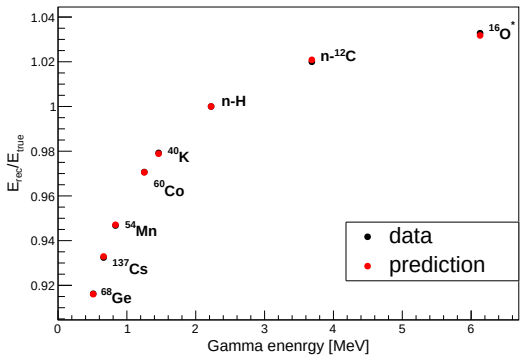

Fig. 1. Fit to data with Eq. (**??**). The black points are data from calibration of gamma, while the red points show the best fit with Eq. (**??**). For ^{60}Co, there two gammas for one calibration event, so the average value 1.25 MeV will be used as the corresponding gamma energy. For neutron captured at ^{12}C, there are one (4.95 MeV) or two gammas (1.26 MeV + 3.68 MeV) with ∼52% and ∼48% branch ratio respectively. So the average energy of gamma with neutron captured at ^{12}C is 3.69 MeV.

The fitted electron physics nonlinearity with the truth obtained from the Geant4 simulation is compared in Fig. **??**, where a good agreement within 1% is obtained.

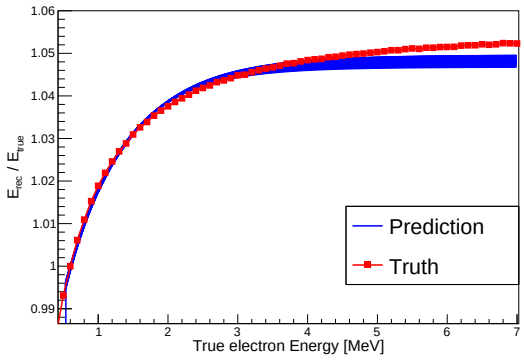

Fig. 2. This figure shows the energy nonlinearity of electron as function of energy. The red points show the truth nonlinearity obtained from simulation, while the blue lines show fit result with gamma source calibration. The blue band is constructed with multiple blue lines considering uncertainty of calibration.

The annihilation gamma response in Eqn. **??** can be directly measured by the ^{68}Ge source. ^{68}Ge decays into ^{68}Ga via electron capture, which then β^+-decay into ^{68}Zn ($T_{1/2}$ =67.7 minutes). Due to the enclosure of the source, positrons will be stopped inside the source, making it effectively a two 511 keV gammas source.

Finally, the thus obtained positron physics nonlinearity (Eqn. **??**) is compared to the true positron nonlinearity in the simulation. in Fig. **??**. The residual bias is less than 0.5% over the entire range of IBD, which is significantly better than our 1% requirement.

2.2 Calibration of Electronics nonlinearity

The nonlinearity of electronics could be calibrated with a laser as a photon source and small PMTs as a monitor. The laser source has a wide range of intensity from hundreds of scintillation photons to millions, which make it possible to calibrate every large PMT from single photon to 50 photons. And the small PMTs have lower detector efficiency compared with large PMTs, but the total small PMTs can be used a monitor for laser intensity since the response is quite linear.

Simulation works...

2.3 Systematic uncertainty analysis

The systematic uncertainty includes optical shadowing effect, Compton effect, statistic effect and electronic nonlinearity effect in analysis. Via simulation we can obtain the corresponding bias for each effect.

2.3.1 Shadowing effect

The shadowing effect is due to the non-transparent or not 100% reflectivity material of source enclosure. The optical photon from energy deposit in LS will be absorbed by the source enclosure.

The source enclosure and weights can be coated with high reflectivity material PTFE to reduce the photon.

In the simulation, the reflectivity of PTFE is assumed 90% as a conservative calculation.

To decouple the shadowing effect and Compton effect, we can only select the events without energy loss. With this selection, the PE spectrum follows the Gaussian distribution, so a full absorption peak is obtained with Gaussian function fit. And then we compare it with the ideal case, "bare" source without enclosure. Fig. **??** shows the bias between "real" and ideal case due to the shadowing effect.

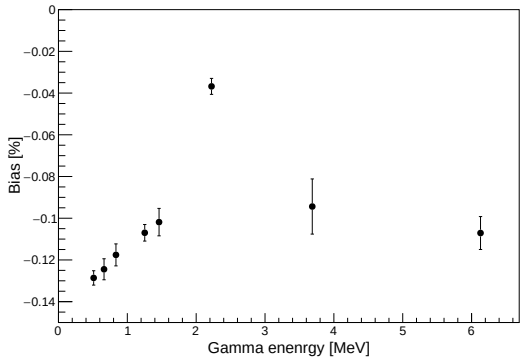

Fig. 3. Optical shadowing effect. The shadow-

ing effect is mainly due to source enclosure and weights. The bias due to the shadowing is less than 0.15% for every source. With the low energy, the bias decreases with energy increase, because the distance of deposit position to source enclosure is bigger for higher energy gamma. However, if the energy it too high, there is some probability that the gamma deposits energy around the weights, which will increase the shadowing effect.

2.3.2 Compton effect

The Compton effect is due to energy loss in the non-LS material, and this will introduce Compton shoulder viewed in PE spectrum. And the Compton shoulder will shift the mean value. Even we use physically-motivated EM calorimeter function in Ref. [**?**] to correct this effect, there is still some uncertainty we should consider. Fig. **??** shows the uncertainty due to the Compton effect. The Fig. **??** shows the simulation of gamma source ^{60}Co with source enclosure. The Compton tail due to energy loss in source geometry will shift the full absorption peak. The fit function will correct the shift.

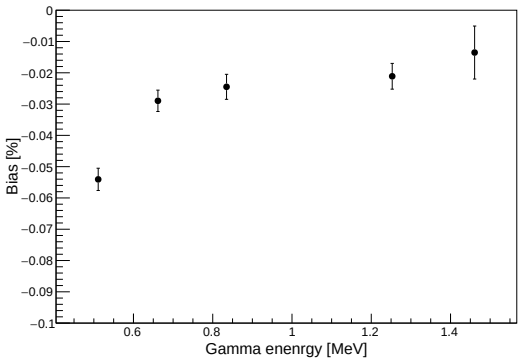

Fig. 4. Compton effect. The Compton effect is also energy dependent. The figure only lists the lower energy cased because that at the higher energy (¿2.22 MeV), there is almost no viewed Compton shoulder with this source geometry.

2.3.3 Electronic effect

Assume the electronic nonlinearity is less than 0.2% after correction.

2.3.4 Statistical effect

The statistical effect is affected by number of calibration events and is energy dependent. The statistical uncertainty should be much smaller than the bias of shadowing and Compton. In this study we control the uncertainty less than 0.01% considering that the shadowing bias is at 0.1% level. As shown in Fig. **??**, the uncertainty is less than 0.01% with $\sim$ 90000 events. It will take about 15 minutes if the rate of source is 100 Hz, which is acceptable for the special calibration.

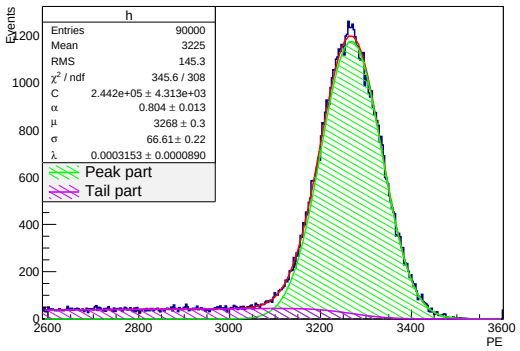

Fig. 5. PE spectrum of ^{60}Co with source enclosure at CD center. Fit the spectrum with physically-motivated EM calorimeter function in Ref.[**?**] to obtain full absorption peak. The μ is full absorption peak of PE spectrum. The tail part of the spectrum can be automatically subtracted during the fitting.

2.3.5 Nuclear recoil smearing for O^{16}

One of the neutron sources is ^{241}Am-^{13}C. The ^{241}Am is an alpha source with kinetic energy $\sim$ 5.5 MeV, and the alpha will be captured by the candidate target ^{13}C. Then the source will produce a neutron with O^{16} in the ground state or excited states. When the O^{16} is at the second excited state, it will emit a 6.13 MeV gamma. The 6.13 MeV gamma can be used for calibration. But at the same time, the nuclear (H and C) will be recoiled by the neutron. The recoiled nuclear will deposit energy in LS, which shifts the energy spectrum of 6.13 MeV gamma and give a positive bias. Based on the MC simulation, the bias is about 0.4%.

2.3.6 Position dependent effect

Since the detector is non-uniform, so the energy scale is also position dependent. Although the non-uniformity can be corrected, the residual bias still exists. In chapter 3, we will comprehensively study the non-uniformity correction and the residual bias shown in Fig. **??**.

2.3.7 Conclusion: energy scale uncertainty $\leq$ 1%

Since all the sources have almost same geometry and electronic system, the corresponding biases are correlated with each other. To study the uncertainty due to the biases, we should generate a random value as a scale, and the bias of every calibration source will be multiply by the same scale as one case of calibration. For shadowing effect, Compton effect and nuclear recoil smearing effect, the random sale will be between 0 and 1 since we exactly know it is a negative bias or positive bias. But for the electronic effect, the random scale should be between -1 and 1 since we won't know if it is positive or negative. For the statistic effect, 0.01% uncertainty will be randomly added to every source without correction

between each other. Repeat above randomly generation, we can get multiple cases of calibration and corresponding reconstruction of positron energy shown in Fig. **??**.

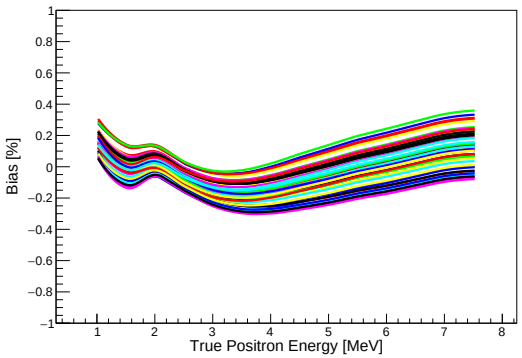

Fig. 6. Systematic uncertainty analysis. The Y axis is the residual bias of positron reconstructed energy and true one after calibration. The different lines show the different cases of calibration with different biases. The overall uncertainty of nonlinearity is less than 1% from 1 to 8 MeV, which meets the physics requirement of MH determination.

3 Minimizing the energy resolution

The energy resolution is dominated by number of photon collected, but worse with non-uniformity and PMT dark noise. To minimize the energy resolution, the non-uniformity should be corrected with the calibration system.

3.1 Formalism(a,b,c)

Referring to ref [**?**], the energy resolution can be parameterized as

$$\frac{\sigma_E}{E} = \sqrt{\left(\frac{a}{\sqrt{E}}\right)^2 + b^2 + \left(\frac{c}{E}\right)^2} \tag{4}$$

where E is the visible energy with the unit of MeV. Parameter a is the statistical term, which is mainly driven by number of photon collected, b is the constant term dominated by the non-uniformity, and c term is mainly due to PMT dark noise. Parameters a and c is the intrinsic property of the detector, which the calibration can't improve, but the constant term b can be reduced with calibration system. Based on Ref.[**?**],the requirement of JUNO energy resolution, better than 3% at 1 MeV, is equivalent to the following equation based on MH sensitivity calculation.

$$\sqrt{(a)^2 + (1.6\times b)^2 + \left(\frac{c}{1.6}\right)^2} \leqslant 3\% \tag{5}$$

The equation shows b is more significant than a, while c is less important than a. So non-uniformity correction with calibration to reduce the constant term "b" can immensely minimize the energy resolution and thereby improve the MH sensitivity.

3.2 Reducing the constant term: non-uniformity correction

Thanks to the spherical design of the JUNO detector, the phi symmetry of the detector make it possible to only calibrate one vertical section to correct the non-uniformity. So a calibration system to deploy the radioactive source in one vertical section is proposed. The locations of calibration source are shown in Fig. **??**. With this strategy, the ratio of detector response in the source location to that of CD center can be obtained. A thin plate spline function is constructed to fit the calibration data to describe the non-uniformity, as shown in Fig. **??**. With algorithm of vertex reconstruction[**?**], vertex of IBD events can be obtained. Then the non-uniformity can be corrected by scaling it to CD center via looking up the corresponding ratio based on the vertex.

In order to value the non-uniformity correction, a simulation is carried out. The mono energy positron uniformly generates in CD.

The full absorption peak and sigma can be obtained with Gaussian function fitting for the mono energy positron spectrum. And the energy resolution can be defined as sigma/mean. The energy resolution will be a standard to evaluate the non-uniformity correction.

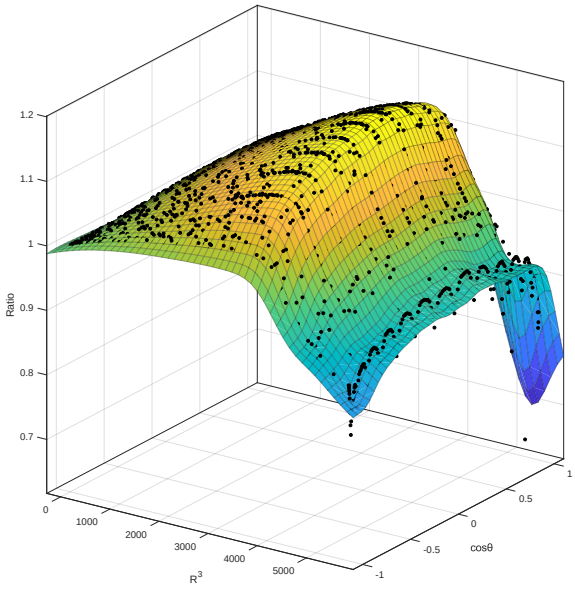

Fig. 7. The non-uniformity response of CD. Z axis is the ratio of PE to that of CD center with same energy source. And X and Y axis is the source locations, R^3 and cosθ.

3.3 Systematics that affect the energy resolution

3.3.1 Ideal case: correction with same energy calibrated

Since the IBD is positron events, so in the ideal case, we should use positron as the calibration source to correct the non-uniformity. And the calibration source should have the same energy as that of IBD events to void energy dependent effect. Ideally, the calibration positions should be infinite but it's impossible even in MC simulation. In this study, $\sim$ 2000 calibration positions will be used for non-uniformity correction. The corrected result is shown in Table??, in which the overall energy resolution is 2.9?%.

3.3.2 Correction with only ^{241}Am-^{13}C (2.22 MeV gamma)

However, there is no mono energy positron source for calibration. So we consider use the neutron source ^{241}Am-^{13}C to correct the non-uniformity of positron. The corrected result is shown in Table??, in which the overall energy resolution is 2.9?%.

3.3.3 Finite calibration points ($\sim$200 points)

Considering realistic case, the calibration points are finite due to limited calibration time and the calibration system design. So the calibration points should be optimized based on energy resolution as shown in Fig. **??**. With the finite calibration points, the energy resolution is worse than before as shown in Table.

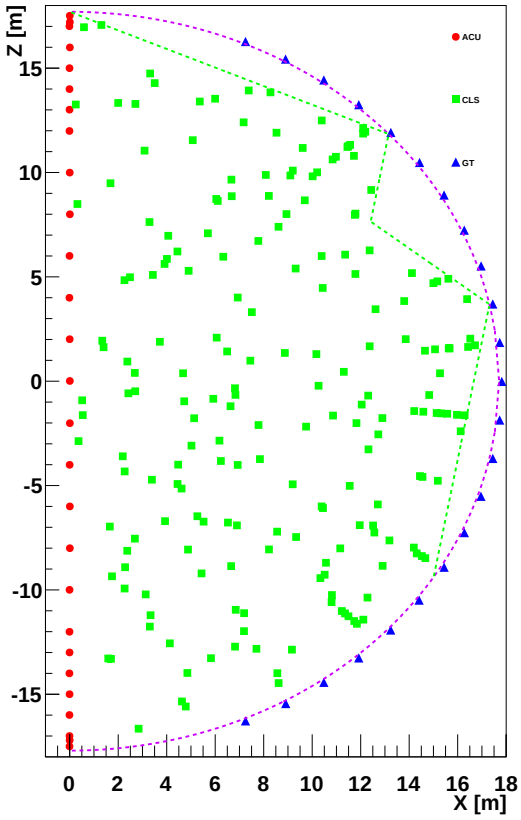

Fig. 8. Basic coverage with ACU, CLS and GT after optimization. Randomly selection from multiple points and choose the best selection with the minimum energy resolution.

3.3.4 Vertex reconstruction

The non-uniformity correction depends on vertex of events, so the vertex reconstruction significantly affects the quality of non-uniformity correction. An algorithm based on time and charge information of PMTs have been developed in Ref. [**?**]. Here we assume 8 cm @1MeV vertex resolution during non-uniformity correction. As shown in table **??**, with the vertex resolution, the overall energy resolution is only 0.02% worse than that without vertex smearing. We also assume different vertex resolution 10 cm/$\sqrt{E(MeV)}$ and 15 cm/$\sqrt{E(MeV)}$, and get corresponding energy resolution 2.94% and 2.96%.

3.3.5 Precision of positioning system

Due to self-weight of cable and friction between anchor and cables, it's difficult to determine the position of the source only based on length of cable. So an independent positioning system was purposed. In this simulation, we assume 3 cm positional accuracy, which is the requirement for the positioning system [**?**]. To simulate this effect, we randomly smear the source position with 3 cm position resolution. With source position smearing during non-uniformity correction, the overall energy resolution is 2.94%, 0.01% worse than before as shown in Fig **??**.

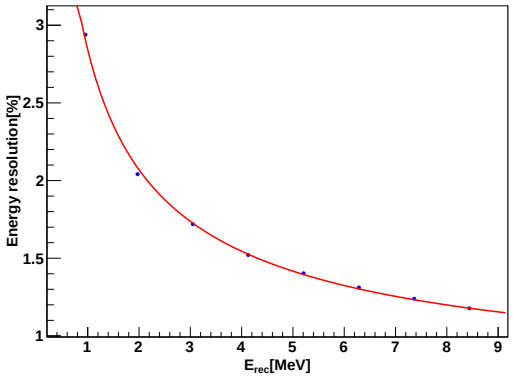

Fig. 9. a=2.75% and b=0.70%, and the overall energy resolution is 2.97% after the non-uniformity correction. The vertex resolution(8 cm @ 1 MeV) and precision of positioning (3 cm accuracy) are considered.

3.3.6 Dark noise

The dark noise of PMT will give additional charge during data taking, called dark hits. Even the value can be subtracted during energy reconstruction with known expected number of dark hits, the uncertainty still increase since the additional dark hits obey Poisson statistics. And the increased uncertainty will worsen the energy resolution. Given the rate of dark noise and certainty time window, the expected value of dark noise is relative constant value, which is energy independent. So as energy increased, the dark noise influence on energy resolution will be decreased. The dark noise effect is corresponding to c term in Eqn. **??**, which not very significant compared with a term and b term. Since the calibration can't improve the energy resolution on c term, so in previous study, we didn't consider the dark noise. But the effect of dark noise can be estimated just based on Poisson statistics. Here we cite the result in [**?**], c = 0.9%, to calculate the overall energy resolution in Eqn. **??**. Table **??** is a summary of energy resolution with different facts including dark noise effect.

3.3.7 Conclusion of energy resolution

The energy resolution can be minimized by correcting non-uniformity correction. In consideration of calibration source, finite points, vertex reconstruction, precision of positioning system and dark noise, the energy resolution will be worse than that of ideal non-uniformity correction, but the overall energy resolution can still reach 3%, which meets the physics requirement. In addition, the mean bias is less than 0.1% after non-uniformity correction, which give very small influence on energy scale uncertainty.

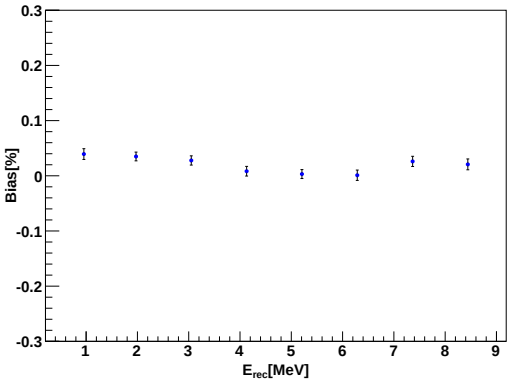

Fig. 10. Mean bias after non-uniformity correction. In the simulation, the mono energy positron from 1 MeV to 8 MeV uniformly distributed in CD. The reconstructed energy will be corrected to CD center based on the corresponding ratio obtain for calibration system. X axis is the energy of positron, while Y axis is the bias between the value at center and that uniformly distributed in CD after non-uniformity correction.

Table 2. Energy resolution with various factors

Effects	a	b	c	$\sqrt{a^2+(1.6b)^2+(\frac{c}{1.6})^2}$
With same energy source	2.693(5)	0.699(5)	0	2.92(1)
With only Am-C	2.693(5)	0.699(5)	0	2.92(1)
Finite calibration points	2.693(5)	0.699(5)	0	2.92(1)
vertex smearing	2.707(6)	0.707(5)	0	2.93(1)
positioning precision	2.75(1)	0.70(1)	0	2.97(1)
dark noise	2.75(1)	0.70(1)	0.9	3.02(1)

4 Design of calibration subsystem

During the calibration, we need deployment systems to move the source to various positions. The deployments systems should cover 1-D, 2-D and 3-D scanning with different calibration frequency. So we propose to use automatic calibration unit (ACU), cable loop system (CLS), guide tube calibration system (GTCS), and remotely operated under-liquid-scintillator Vehicles (ROV) as shown in Fig **??**. For ROV and CLS, we will use independent positioning system to determine the position of calibration source.

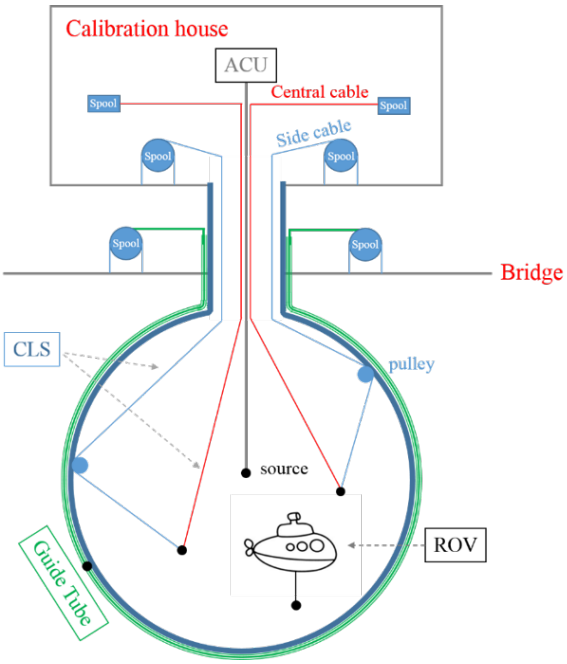

Fig. 11. The overview of calibration system, including automatic calibration Unit (ACU), cable loop system (CLS), Guide Tube (GT) and Remotely Operated Under-liquid-scintillator Vehicles (ROV)

4.1 Automatic Calibration Unit (ACU)

The ACU is developed to do calibration along the central axis of CD, which is very similar to the ACU in Daya Bay experiment [**?**]. There are 4 spools installed on the turntable. Three routine sources and one temperature sensors are installed on the ACU. The three routine sources include one gamma source, one neutron source (Am-C) and one laser source. The calibration with ACU can coverage central axis of CD, with high precision of position control. The energy scale of CD can be used with neutron source deployed by ACU to the CD center.

4.2 Cable loop system (CLS)

The CLS could deploy the calibration source in one vertical section in the CD. The CLS mainly consist of two cables, side cable and central cable. Controlling the lengths of two cable, we can deploy the sources to scan one vertical section area. Two sets of CLS with different anchor positions are purposed to increase the scanning area.

4.3 Guide Tube Calibration System (GTCS)

Since the source cannot reach some boundary area of CD duo to mechanical limit, a guide tube calibration system was purposed. The guide tube will be out of CD. With the GTCS, we can position the calibration source along the surface of CD to get better understand of boundary effect.

4.4 Remotely Operated Under-liquid-scintillator Vehicles (ROV)

ROV is a 3D scanning system, meaning that we can move the calibration source to nearly everywhere in the CD. ROV is not a routine calibration system, but it still essential as a supplement of ACU, CLS, and GT.

4.5 Positioning system

During the non-uniformity correction, we should precisely know the position of calibration points, so it's very important to get the position of calibration source. However, it's difficult to determine position of source only based on length of cable. Due to self-weight, the cable is not straight, so it is difficult to calculate the position of source with naive trigonometric relation. So it's necessary to use independent position system to determine the source position. The requirement of precision of source position is ∼3 cm [**?**] compared with that the requirement of vertex reconstruction is ∼10 cm [**?**].

5 Calibration program

The conceptual calibration strategy is based on above simulation result. The rate of the radioactive source is about 100 Hz since it's difficult to make lower radioactive source and limited by bandwidth of data transmission, the rate can not be very high. To ensure uncertainty less than 0.1%, 1 minutes calibration for one position is enough with more than 5000 calibration events. The source moving time should also be considered, since with the huge size detector, it will take a lot of time for source moving during every calibration. In consideration of safety, the speed of source moving is limited at 1 m/minutes. The calibration includes special calibration only one time at the beginning and routine calibration every week or every month. The routine calibrations can be divided into two parts, weekly calibration and monthly calibration.

5.1 Special calibration

The special calibration can be carried out at the beginning of physics data taking for the nonlinearity and non-uniformity correction. In this calibration, multiple sources at CD center will be used for nonlinearity correction and source also will be deployed at many locations for non-uniformity correction. It will take relative much time for the calibration to have a better understanding of CD including energy nonlinearity and non-uniformity, as shown in Table **??**. The neutron source Am-C will be used for both non-uniformity correction and nonlinearity correction. Other sources will only be used for nonlinearity correction at CD center.

5.2 Weekly calibration

The weekly calibration will be operated every week with one radioactive source and one laser source, as shown in table **??**. The weekly calibration can monitor the variation of energy scale in both physics and electronics. During the weekly calibration, only ACU will be executed since the source will be only positioned at CD center.

5.3 Monthly calibration

The monthly calibration will be operated every month. During the monthly calibration, the ACU, CLS, and GT will be operated as shown in table **??**. One vertical section of the CD will be scanned with the calibration source. It will take too much time and bandwidth of data transmission if we scan all 251 points. So considering time and data transmission, we propose to just select 40 typical points in CLS calibration to monitor the non-uniformity.

Table 3. Time of special calibration

Source	Energy [MeV]	Points	Travel time [min]	Date taking time [min]	total time [min]
Neutron (Am-C)	2.22	251	350	1225	/
Laser	/	6	67	36	103
^{68}Ge	0.511×2	1	27	15	/
^{137}Cs	0.662	1	27	15	/
^{54}Mn	0.835	1	27	15	/
^{60}Co	1.17+1.33	1	27	15	/
^{40}K	1.461	1	27	100	/
Total	/	/	512	1421	1933 (∼32 h)

Table 4. Time of weekly calibration

Source	Energy [MeV]	Points	Travel time [min]	Date taking time [min]	total time [min]
Neutron (Am-C)	2.22	5	27	5	32
Laser	/	6	27	36	63
Total	/	/	54	31	85 (∼1.5 h)

Table 5. Time of monthly calibration

System	Source	Points	Travel time [min]	Date taking time [min]	total time [min]
ACU	Neutron (Am-C)	21	54	21	75
CLS	Neutron (Am-C)	40	160	40	200
GT	Neutron (Am-C)	11	40	11	51
Total	/	/	/	/	326 (∼5.5 h)

6 Conclusion

In this study, a JUNO calibration strategy was proposed, including the calibration sources, design of calibration deployment system, and the expected results. Based on the MC simulation, the calibration system is able to meet the physics requirements, energy resolution less than 3%, and uncertainty of energy scale less than 1%.

Appendices A

References

1 Fengpeng An et al. 2016 . Phys. G: Nucl. Part. Phys. 43 030401
2 Li Y F, Cao J, Wang Y and Zhan L 2013 Phys. Rev. D 88 013008
3 M. Tanabashi et al. (Particle Data Group) 2018 Phys. Rev. D 98, 030001
4 Agostinelli S et al. (GEANT4) 2003 Nucl. Instrum. Meth. A506 250-303
5 JUNO Collaboration (Lin, Tao et al.) J.Phys.Conf.Ser. 898 (2017) no.4, 042029 arXiv:1702.05275
6 D.J. Griffiths (1987). Introduction to Elementary Particles. Wiley. ISBN 0-471-60386-4
7 F. P. An et al. 2014 Phys. Rev. Lett. 112, 061801
8 Jia-Hua Cheng et al. arXiv 1603.04433
9 Y. Zhang et al. 2019 JINST 14 P01009
10 Q. Liu et al 2018 JINST 13 T09005
11 Ultrasonic Positioning System for the Calibration of JUNO Detector
12 H X Huang et al 2013 JINST 8 P09013